Reaction of Lithium Amide with Methane. An ab Initio and Atoms in Molecules Study

ARTICLE *in* THE JOURNAL OF PHYSICAL CHEMISTRY · APRIL 1993

Impact Factor: 2.78 · DOI: 10.1021/j100117a017 · Source: OAI

5 AUTHORS, INCLUDING:

Richard Dixon
University of California, Berkeley
6 PUBLICATIONS **60** CITATIONS
SEE PROFILE

Andrew Streitwieser
University of California, Berkeley
116 PUBLICATIONS **3,467** CITATIONS
SEE PROFILE

Reaction of Lithium Amide with Methane. An ab Initio and Atoms in Molecules Study

Richard E. Dixon,[†] Andrew Streitwieser,*[,†] Keith E. Laidig,[‡] Richard F. W. Bader,*[,‡] and Sjoerd Harder[†]

Departments of Chemistry, University of California, Berkeley, California 94720, and McMaster University, Hamilton, Ontario L8S 4M1, Canada

Received: December 18, 1992

The reaction of lithium amide with methane was studied with ab initio calculations, and the electron density function was analyzed using the theory of atoms in molecules. The transition state for the reaction is a highly ionic species that can be modeled approximately as an ionic aggregate. The nature and evolution of the bonds were monitored throughout the reaction and related to the accompanying changes in the behavior of the charge density at the bond critical points and in the properties of the individual atoms. The contributions of each atom to the energies of reaction and activation were determined. The HF/6-31G* level of theory was tested by an MCSCF calculation of the transition state and shown to perform adequately in the description of the reaction. The effect of solvation was studied by the addition of molecule of ammonia.

Introduction

One of the important reactions in synthetic organic chemistry is that of metalation, usually by an alkyllithium or lithium amide reagent, followed by reaction of the intermediate organolithium species with a desired electrophile.[1] The reaction is generally carried out in nonpolar ether solvents, such as tetrahydrofuran, in which the reagents are present predominantly as ion pairs and aggregates. Thermodynamic considerations of relative equilibrium acidity are generally important in such reactions, but kinetic effects frequently play an important role. A continuing problem in physical organic chemistry is the characterization of transition states in such ion pair proton transfer reactions and the effects of structure on their relative energies. To this end ab initio molecular orbital (MO) calculations can provide a useful tool, particularly since solvation effects on such ion pair reactions, in which the transition state has no net charge, are not expected to have effects of the same magnitude as corresponding ionic reactions.

In the study of weak carbon acids, kinetic acidities are especially important. A number of proton-exchange kinetics have been reported for reactions of alkanes and cycloalkanes with cesium cyclohexylamide in cyclohexylamine solution.[2] Cesium cyclohexylamide is far too large for practical ab initio calculations; thus, lithium amide was considered instead. Subsequent papers will show that this simple model works rather well in correlating experimental reactivities. As a first step in the computational study of $LiNH_2$ with a series of hydrocarbons, a thorough exploration was made of its reaction with methane. The subsequent studies with larger hydrocarbons will compare the calculated reaction barriers to measured relative rates with the objective of determining whether a Brønsted correlation derived in this way will permit the conversion of kinetic acidities to equilibrium ion pair acidities. Since relatively large hydrocarbons will be involved, an important objective of the present work was to find the lowest level of theory that would adequately describe the systems to be considered. We also examine in greater detail the proton-transfer reaction for the case of methane on the assumption that the other hydrocarbons to be considered react by the same mechanism.

Kaufmann et al.[3] have presented computations of the symmetrical hydrogen exchange reactions between lithium and sodium compounds MY and the corresponding hydrides YH and a related study of reactions of LiH with methane and acetylene. In general, the reactants form an association complex MY·HY, which is more stable than the separated reactants before proton transfer. Accordingly, we have computed the model reaction as involving two association complexes, Ia and Ib, and a proton-transfer transition state, It:

$$\underset{}{LiNH_2 + CH_4 \rightarrow} \underset{\text{Ia}}{LiNH_2\cdot CH_4} \rightarrow \underset{\text{It}}{[Li^+(H_2N\cdot\cdot H\cdot\cdot CH_3)^-]^\ddagger} \rightarrow \underset{\text{Ib}}{H_3N\cdot LiCH_3} \rightarrow CH_3Li + NH_3 \quad (1)$$

The absence of solvation provides a large computational simplification but also a substantial difference from experiment. Accordingly, we have additionally studied the effect of including one solvent molecule in the transition state, IIt:

$$\underset{}{H_3N\cdot LiNH_2 + CH_4 \rightarrow} \underset{\text{IIa}}{H_3N\cdot LiNH_2\cdot CH_4} \rightarrow \underset{\text{IIt}}{[H_3N\cdot Li^+(H_2N\cdot\cdot H\cdot\cdot CH_3)^-]^\ddagger} \rightarrow (H_3N)_2\cdot LiCH_3 \rightarrow CH_3Li\cdot NH_3 + \underset{\text{IIb}}{NH_3} \rightarrow CH_3Li\cdot NH_3 + NH_3 \quad (2)$$

We also include calculations with sodium as a counterion to model the trends in going from lithium to cesium.

Methodology

All geometries were fully optimized within the designated symmetry constraints at the restricted Hartree–Fock[4] level of theory using gradient optimization techniques[5] and the standard 6-31G* and 6-31G** basis sets incorporated into the GAUSSIAN 86 and 88[6] and GAMESS[7] program systems. Frequency analyses were carried out with the 6-31G* basis set to characterize stationary points. Some of the starting structures were taken from the Carnegie-Mellon Quantum Chemistry Archive.[8] A potential energy surface walking algorithm[9] incorporated into GAMESS enables one to determine and follow the reaction coordinate in a stepwise manner by proceeding downhill toward both reactants and products from the maximum on the potential energy surface with the initial steps being dictated by the atomic displacements for the mode with the imaginary frequency. This procedure was employed in the present investigation. The properties of the atoms and the determination of the structures and their properties along the reaction path were obtained using

[†] University of California, Berkeley.
[‡] McMaster University.

0022-3654/93/2097-3728$04.00/0

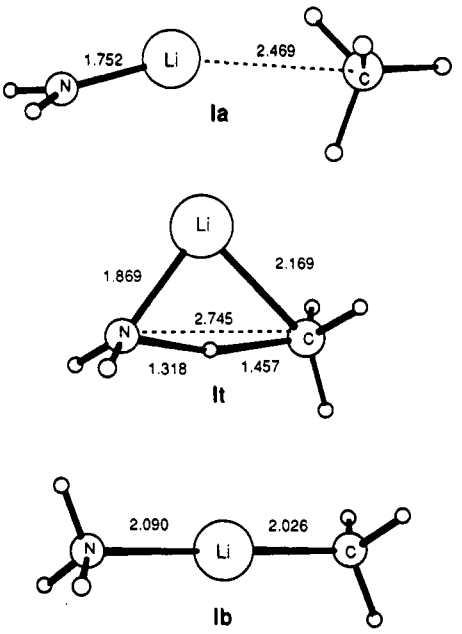

Figure 1. Initial association complex, Ia, transition state, It, and post-transition-state complex, Ib, for the reaction of methane with lithium amide, eq 1.

the program PROAIM.[10] For the present purposes zero-point energy corrections were not applied.

Performance of the Hartree–Fock Model

The critical structure on the potential energy surface for the reaction considered is the transition state, since the partial bonds in it must be described correctly. Figure 1 shows the transition state for the reaction of methane with lithium amide, It, at the Hartree–Fock 6-31G* level of theory. Note that in the transition state the transferred proton is situated roughly equidistant from carbon and nitrogen. The carbanion "fragment" is strongly stabilized by bonding to the lithium atom; the C–Li bond distance is almost as short as that in methyllithium. Vibrational analysis of the transition-state structure results in one imaginary frequency. The vibration associated with that frequency corresponds to the motion of the transferred proton between carbon and nitrogen; the structure is thus the transition state for the reaction we are interested in and not for some different process, in which case the imaginary frequency would correspond to a different type of motion, for example, a methyl rotation. Similar structures were found by Kaufmann et al.[3] for the symmetrical transition states of LiX + XH, although in the reaction of LiH with methane the C–H–H bond is almost linear. The bent structure of the transition state can be rationalized in terms of an electrostatic model by considering the carbon and nitrogen as negative point charges, and the proton and lithium as positive point charges. The arrangement of these point charges is most stable in a configuration analogous to that of this transition state.[11]

The ability of a given level of theory to describe the methane/lithium amide transition state was evaluated by observing the changes in structure and energy of the transition state upon improvement of the level of theory. In their studies, Kaufmann et al.[3] found little difference in relative transition-state energies between 6-31G* and higher basis sets. Thus, the initial level used in the present study was HF/6-31G*. Because the transferred proton is involved in two partial bonds in the transition state, the use of additional functions to describe electrons in the vicinity of this proton could perhaps produce significant changes. Table I shows that the use of 6-31G**, with the addition of p functions on hydrogen, has no significant effect on the structure of the transition state. Optimization with the 6-31G** basis set slightly shortens the bond to carbon of the proton being transferred from 1.457 to 1.450 Å, and the angle between the transferred proton, carbon and lithium is decreased by 0.2°. These small changes indicate that the 6-31G* basis set adequately describes the structure of the transition state in agreement with the results of Kaufmann et al.[3]

TABLE I: Comparison of Structural Features for the Transition State (It) of the Reaction of Methane with Lithium Amide with Variation of the Basis Set and with Inclusion of Second-Order Perturbation Theory

parameter[a]	HF/6-31G*[b]	HF/6-31G**	MP2(FU)/6-31G*
energy, hartrees	−103.191 913 6	−103.209 769 1	−103.536 106 2
N2–C1	2.745	2.740	2.752
Li3–C1	2.169	2.163	2.138
H4–C1	1.457	1.450	1.472
H6–C1	1.097	1.097	1.102
H5–C1	1.088	1.088	1.094
H4–N2	1.318	1.318	1.315
C1–H4–N2	163.21	163.76	161.87
H5–C1–N2	105.67	105.54	103.96
H4–C1–Li3	50.70	50.52	51.41
H6–C1–Li3	92.82	92.88	93.53
H6–C1–Li3–N2	126.52	126.54	126.33
Li3–C1–N2	42.73	42.79	42.86

[a] Bond lengths in angstroms, bond angles in degrees. Numbers correspond to the Z matrices that are available from the first senior author. [b] MP2(FC) −103.526 27; MP2(FU) −103.535 59.

The second aspect of the evaluation of a level of theory for this study concerns electron correlation, which has been shown in some other cases to have large effects on structure, especially when partial bonds are involved.[12] Similarly, in their study, Kaufmann et al.[3] found that correlation effects at the MP2 level have a significant effect on relative transition state energies but little effect on structure. We also carried out a full geometry optimization of the transition state using second order many-body perturbation theory (MP2(FU)/6-31G*). The results summarized in Table I shows that this optimization has only a small effect on the geometry of the transition state. The proton-carbon bond distance is increased by 0.02 Å, and the proton–carbon–lithium angle is increased by 0.7° compared to Hartree–Fock optimization. The difference in energy of the two transition-state structures, MP2//6-31G* vs MP2//MP2 (both full MP2), is only 0.35 kcal mol^{-1}. In particular, there is no significant change in the region of the transferred proton, a feature of the transition states of particular concern.

These results suggest that weak covalent bonds do not dominate the transition state; that is, the transition state has much of the character of a quadruple ion. In a quadruple ion the interactions are effectively among closed shells and mutual correlation is less important. The MP2 result found suggests that HF optimized structures for larger hydrocarbons will also be close to the MP2 optimized structures, and we can thus deal only with structures optimized at the Hartree–Fock level. However, we thought it important to more fully test the role of correlation. Although the MP perturbation approach can provide an important test, it is still based on a single Slater determinant. Accordingly, a multiconfigurational SCF (MCSCF) calculation[13] was carried out with the 6-31G* basis set. For this calculation, 4627 configurations (allowing a maximum of 6 simultaneous electron excitations) were considered. The resulting MCSCF wave function consists almost entirely (98.3%) of the ground-state configuration, indicating that configurations above the reference configuration do not contribute significantly to the wavefunction and that the transition state does not have significant diradical character.

Counterion and Solvation Effects

Additional calculations for the transition state of the reaction of lithium amide with methane were done in which a molecule of ammonia of solvation, IIt, no counterion, IIIt, and a larger

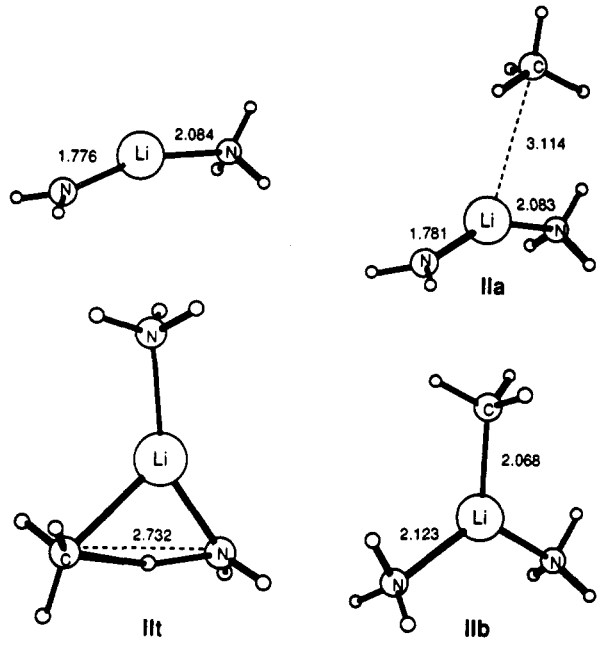

Figure 2. Lithium amide and the initial association complex, IIa, transition state, IIt, and post-transition-state complex, IIb, solvated with one molecule of ammonia, eq 2.

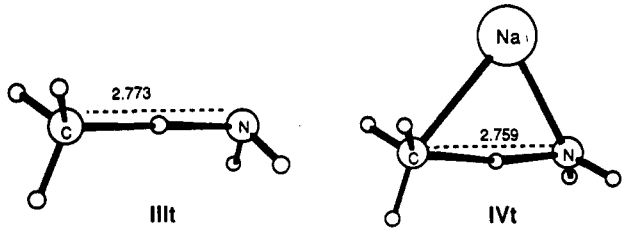

Figure 3. Transition states for the reactions of methane with amide anion, IIIt, and with sodium amide, IVt.

counterion (sodium), IVt, were used. Variations in the structure of the transition states with counterion could then perhaps be correlated with experimental counterion effects. The inclusion of an extra molecule of ammonia permits an assessment of the role of solvation. The transition states for these reactions are included in Figure 2 and 3. Structural parameters for the four transition states are summarized in Table II.

From Figures 1–3, it can be seen that the carbon–nitrogen distance is almost invariant in all cases. In structures It, IIt, IIIt, and IVt the C–N distance varies only from 2.74 to 2.77 Å. In the ionic transition state IIIt with no counterion, the carbon, the transferred proton and the nitrogen are now almost in line ($\angle$(C–H–N) = 178.6°). In the quadruple ion transition states this angle is more bent: It, 163.2°, IIt, 164.8°, IVt, 169.0°. Solvating or replacing the lithium by a larger cation results in a progressive increase in this bond angle toward linearity. This result can also be rationalized in terms of electrostatics of an ionic model or highly polar transition state. In general, the fragments of the transition state that are directly involved in the proton transfer do not change much, most of the change being in the attached methyl and amide proton fragments. Although lithium has not reached its usual four-coordinated state in the solvated structure, the present results suggest that only minor changes would result from additional coordination.

Reactant and Product Complexes

As in the Kaufmann et al. examples,[3] reaction of lithium amide with ammonia first gives a loose complex, Ia (Figure 1). This complex has C_S symmetry and the two components have virtually unchanged geometries. This polarization complex is only 3.4 kcal mol^{-1} more stable than the reactants at 6-31G*. This energy difference diminishes to 1.2 kcal mol^{-1} at 6-31G**. With a molecule of ammonia of solvation the complex IIa is now only 0.9 kcal mol^{-1} more stable than the reactants; the potential surface is extremely flat and the resulting complex now has C_1 symmetry (Figure 2). This result suggests that with additional solvation the complex would essentially disappear. As shown in Figure 4, solvation has only a small effect on the barrier height to the transition state. That is, solvation of lithium by a single solvent has about the same effect on the transition state as on lithium amide.

Transition state It leads to methyllithium solvated by ammonia, Ib (Figure 1).[14] This process is less exothermic when an additional molecule of ammonia of solvation is included. As summarized in Figure 4, solvation of methyllithium by the first ammonia is exothermic by 24.1 kcal mol^{-1}, whereas a second ammonia provides only 14.2 kcal mol^{-1} more. The overall reaction from reactants to separated products is endothermic by 23.4 kcal mol^{-1} at 6-31G*; this value is 22.0 kcal mol^{-1} at 6-31G**. With one ammonia of solvation the endothermicity is 22.9 kcal mol^{-1} at 6-31G* (Figure 4). The slight increase in solvation energy of methyllithium relative to lithium amide, 0.5 kcal mol^{-1}, is consistent with the longer C–Li bond distance in the former compared to the N–Li distance in the latter. The solvation energy of the first ammonia is remarkably constant for all of the species shown in Figure 4. This constancy was noted by Kaufmann et al.[14] in their study of solvation energies of first row lithiated species. These authors also made an extensive study of basis set effects and included zero-point energy corrections.

An Electron Density View of the Reaction Pathway

In addition to structural changes occurring during the course of reaction it is instructive to examine the changes in the electron density function. The topology of the electron density function, ρ, at 6-31G** was examined with the use of zero flux surfaces and bond critical points in the theory of atoms in molecules (AIM).[15] The interaction of two electron density distributions leads to the formation of a bond critical point in ρ, the charge density. Two gradient vectors of ρ originate at this point and trace out a line, the bond path, linking the nuclei of the two atoms along which the electron density is a maximum with respect to any neighboring line. The collection of bond paths defines the molecular graph for a given geometry and all geometries possessing equivalent molecular graphs possess the same molecular structure.

The course of the reaction is summarized by the sequence of molecular graphs shown in Figure 5. Note that these structures are generally not stationary points on the potential energy surface. The process starts with structure **1**, which is slightly along the reaction path from the initial complex Ia in a region where the potential energy surface is rather flat. The geometries of structures **2** and **3**, which evolve from **1**, have molecular graphs equivalent to **1** and represent the same general molecular structure. The progressive shortening and strengthening of the hydrogen bond to the nitrogen atom is paralleled by a progressive lengthening and weakening of the original bond to carbon. There is an abrupt change in structure between **3** and **4** with the formation of a bond between carbon and lithium to give the ring structure found in the transition state. This change in structure does not occur until the energy of the reactant structure has increased to within $\approx$1 kcal mol^{-1} of the top of the barrier. The ring structure persists until the reaction is nearly complete, the final open structure of the product complex being obtained with the severing of the original C–H bond.

The bonded ring of atoms is the result of the formation of an unstable critical point in ρ between the C and Li nuclei, a critical point with a zero curvature in ρ, which bifurcates into a bond and a ring critical point, the latter denoted by a triangle in Figure 5. This newly formed ring critical point first appears adjacent to the position of the C–Li bond critical point for an infinitesimal motion

TABLE II: Variation of Structure of the Transition State for the Reaction of Methane with Lithium Amide upon Change of Counterion and Solvation, HF/6-31G*

parameter	lithiated (It)	sodiated (IVt)	solvated (IIt)	ionic[a] (IIIt)
energy, hartrees	−103.191 91	−257.572 03	−159.412 50	−95.665 97
H4–C1–M3	50.7	54.29	50.84	42.08
H5–C1–N2	105.67	106.84	107.41	112.95
H6–C1–M3	92.82	88.7	91.11	88.32
H8–N2–M3	125.93	126.53	126.04	126.87
H5–C1	1.088	1.089	1.089	1.101
H6–C1	1.097	1.100	1.098	1.100
N2–C1	2.745	2.759	2.743	2.773
H6–C1–M3–N2	126.52	126.81	126.68	127.02
H8–N2–M3–C1	97.59	98.23	97.35	76.81
H8–N2	1.005	1.007	1.006	1.017
H4–C1	1.457	1.464	1.466	1.442
M3–C1	2.169	2.514	2.222	
M3–C1–N2	42.73	49.08	43.71	
M3–N10			2.076	
H11–N10			1.005	

[a] A dummy atom was substituted for the counterion to keep the definition of geometrical parameters.

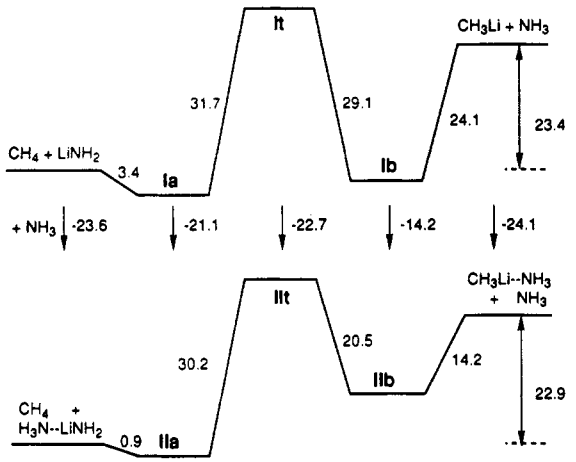

Figure 4. Energetics of the reaction sequence (6-31G*) without, I, and with, II, one molecule of ammonia of solvation. Energies (au) not given in Tables I and II are CH_4, −40.195 17; $LiNH_2$, −63.041 95; Ia, −103.242 50; Ib, −103.238 24; CH_3Li, −47.015 54; NH_3, −56.184 36; $H_2NLi{\cdot}NH_3$, −119.263 97; IIa, −159.460 55; IIb, −159.445 21.

past the bifurcation geometry, a geometry just preceding that in structure **4**. The proximity of the newly formed bond and ring critical points in **4** is reflected in the very large value of 9.4 for the ellipticity of its C–Li bond.[15,16] The ring critical point migrates away from this newly formed bond toward the C–H bond critical point as this latter bond is lengthened and the N–H bond is shortened. At an energy close to that of the products, the ring critical point coalesces with the C–H bond critical point and the C–H bond is broken. This process, which occurs for a geometry intermediate between that for structures **10** and **11**, is the reverse of that leading to the formation of the C–Li bond. A positive curvature of the ring critical point annihilates the negative curvature of the C–H bond critical point lying in the ring surface to yield a critical point with one zero curvature. This unstable critical point vanishes for a further motion along the reaction coordinate yielding the open structure shown in **11**.

Thus the formation, migration, and destruction of the ring critical point, the point where the electronic charge density attains its minimum value in the surface of the ring, determines the fate of the transition-state structure.[15] An atomic view of the structural changes depicted by this series of molecular graphs is obtained through a study of the accompanying changes in the properties of the atoms and of the bonds that link them.

Atomic and Bond Properties of the Reactants and Products

The set of trajectories of ρ that terminate at a bond critical point defines the interatomic surface which separates the basins of a pair of neighboring atoms. The surface is not crossed by any trajectories of $\nabla\rho$ and an atomic surface is one of zero flux in the gradient vector field of the charge density. An atom's basin is bounded by such surfaces and, as a consequence, its properties are defined by quantum mechanics. An atomic population, $N(\Omega)$, is obtained by integrating the charge density over the basin of atom Ω. Its atomic charge $q(\Omega) = Z_\Omega - N(\Omega)$, where Z_Ω is the nuclear charge.

Shown in Figure 6 are contour plots of the charge distributions overlaid with bond paths and the intersections of the interatomic surfaces for points along the reaction path. Table III gives the atomic charges and the changes in the atomic charges and atomic energies, $\Delta N(\Omega)$ and $\Delta E(\Omega)$, for the reactant and product molcules. The features of the charge distributions to be discussed for the reactants and products are evident in the distributions shown for their initial and final adducts in **1** and **12** (**12** corresponds to Ib). There is a small transfer of charge from carbon to each hydrogen in methane, while in methyllithium the carbon as well as the hydrogens bear significant negative charges, the lithium transferring 90% of its valence density to methyl. As a result, the carbon and hydrogen atoms of methyl are stabilized in the product molecule. The charge distribution in methyllithium has been discussed frequently and it is well known that there is a considerable transfer of charge from lithium to carbon.[17]

In ammonia there is a transfer of charge from hydrogen to nitrogen. In lithium amide 93% of the valence density of lithium is transferred to the NH_2 fragment. Unlike the case with the less electronegative carbon in methyl, most of this charge is transferred to nitrogen. Although the nitrogen atom undergoes a considerable loss of electronic charge in forming the product NH_3, the binding energy per electron for the nitrogen atom, the quantity $E(\Omega)/N(\Omega)$, is significantly more negative in the product than in the reactant molecule and the nitrogen atom is stabilized in the products. The increase in the tightness of the binding of the nitrogen charge density in ammonia over that found in the amide is evident in the corresponding displays of the charge distributions. As discussed below, in the reactant amide there are two nonbonded charge concentrations on nitrogen, while in the product ammonia there is but one.

The largest changes in atomic properties are found for the hydrogen atom transferred from carbon to nitrogen in exchange for lithium. The loss of 0.43 electronic charges results in a large increase in its energy. The lithium, on the other hand, undergoes only a small gain in charge and a corresponding small decrease in energy, as it switches its ionic binding from N to C.

The properties of ρ at a bond critical point summarize the nature of the bond. The value of the electron density at the critical point, the quantity ρ_b, provides a measure of bond order. For the interaction between a given pair of atoms, the value of

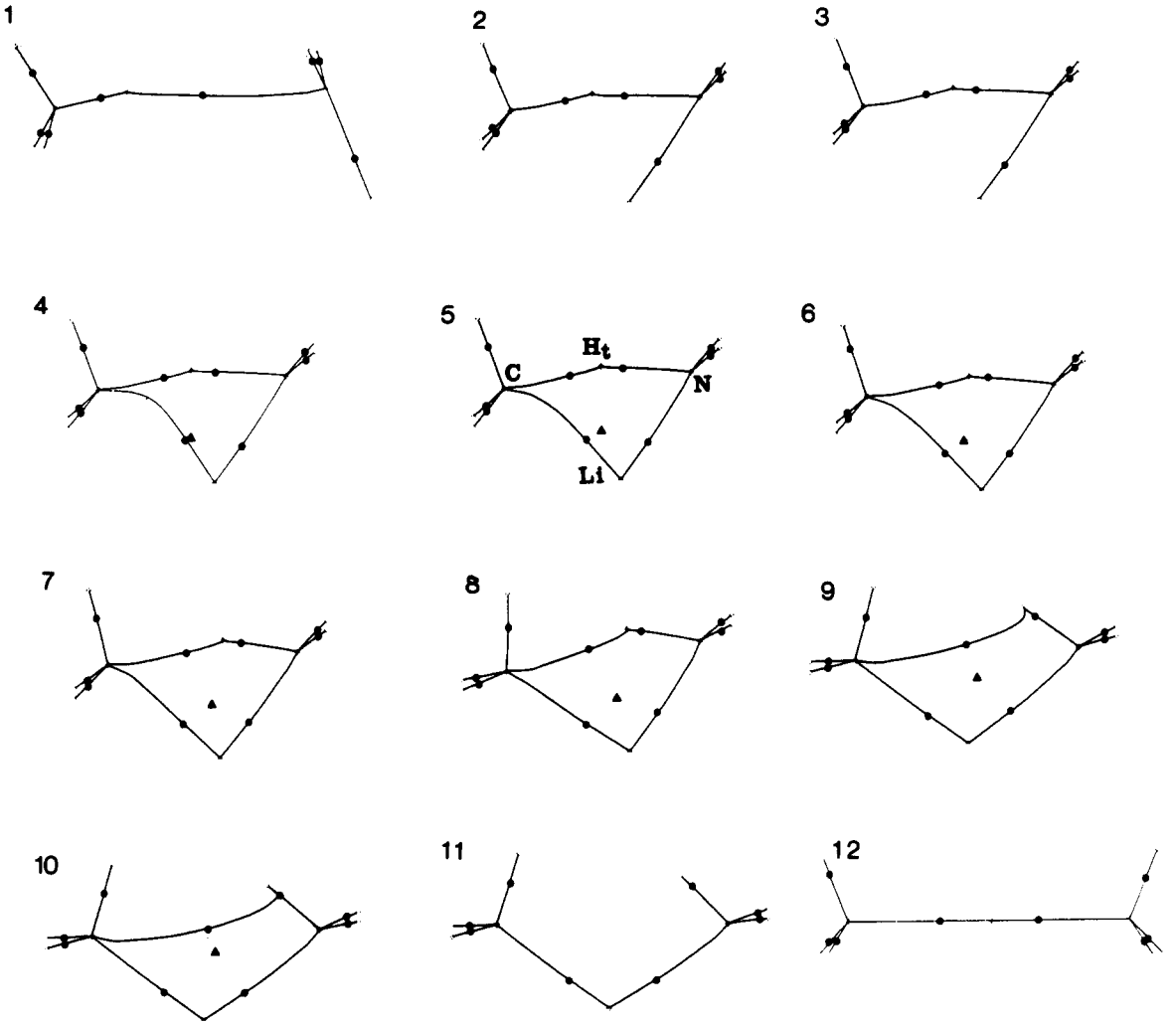

Figure 5. Molecular graphs showing the theoretically determined structures and changes in structure along the reaction path. The relative energies are given in Table IV. The ring critical point is denoted by a triangle. Nuclear positions are denoted by crosses and out-of-plane nuclei by open crosses. The C–Li bond is formed at a geometry just preceeding structure **4** and the C–H bond is broken immediately following structure **10**.

ρ_b increases as the bond length decreases and the strength of the interaction increases.[15,18] The curvature of ρ at a given point determines whether electronic charge is locally depleted (curvature positive) or locally concentrated (curvature negative) at the point in the sense that for a positive curvature, the value of ρ at the point is less than its value averaged over neighboring points, with the reverse being true for a negative curvature. The sum of the three curvatures of ρ defines the Laplacian of the electron density, the quantity $\nabla^2\rho$. The electron density is a maximum at a bond critical point in the interatomic surface and electronic charge is locally concentrated there, as the two curvatures of ρ in the surface that are perpendicular to the bond path are negative. The electron density is a local minimum at the critical point along the bond path, as the third curvature is positive and charge is locally depleted at the critical point with respect to neighboring points along the bond path. Thus, the formation of an interatomic surface and a chemical bond is the result of a competition between the perpendicular contractions in ρ which lead to a concentration or compression of electronic charge towards and along the bond path and the parallel expansion of ρ away from the interatomic surface which leads to its separate concentration in one or both of the atomic basins. The sign of $\nabla^2\rho_b$ determines which of the two competing effects dominates a given interaction.[15,19] As a consequence of the appearance of the Laplacian of ρ in the local expression for the virial theorem, it can be shown that the potential energy dominates the local electronic energy and is stabilizing in those regions of space where the Laplacian is negative and electronic charge is concentrated.[15,19] The values of ρ_b and $\nabla^2\rho_b$ for the reactant and product bonds are given in Table III and the Laplacian distributions along the reaction path are displayed in Figure 7.

The values of $\nabla^2\rho_b$ and the displays of the Laplacian distributions for structures **1** and **12** show that C–H and N–H interactions in methane and ammonia or in their lithium derivatives are dominated by the perpendicular contractions of the charge density towards the bond path, leading to a shared concentration of electronic charge in their internuclear regions. The charge concentrations in the valence shells of the carbon and nitrogen atoms are contiguous with the charge concentrations in the protons, Figure 7. As a consequence, the corresponding values of ρ_b are large. These are shared interactions: the nuclei are bound by the electronic charge that is both accumulated and concentrated in the internuclear region.

The interactions with the lithium atom are representative of the other extreme of atomic interaction, one which is dominated by the positive curvature of ρ, leading to the separate concentration of electronic charge in one or both of the atomic basins. The Laplacian distributions indicate that the considerable transfer of charge that occurs when a lithium atom combines with a methyl or an amide group results in the loss of its valence shell charge concentration. The characteristics of these interactions are those of the closed-shell limit: $\nabla^2\rho_b$ is positive and ρ_b is relatively small in value, a result of the removal of charge from the region of the interatomic surface, as required for the approach of two systems each of which approaches the spin paired limit. In these systems, both nuclei are bound by the electronic charge concentrated in

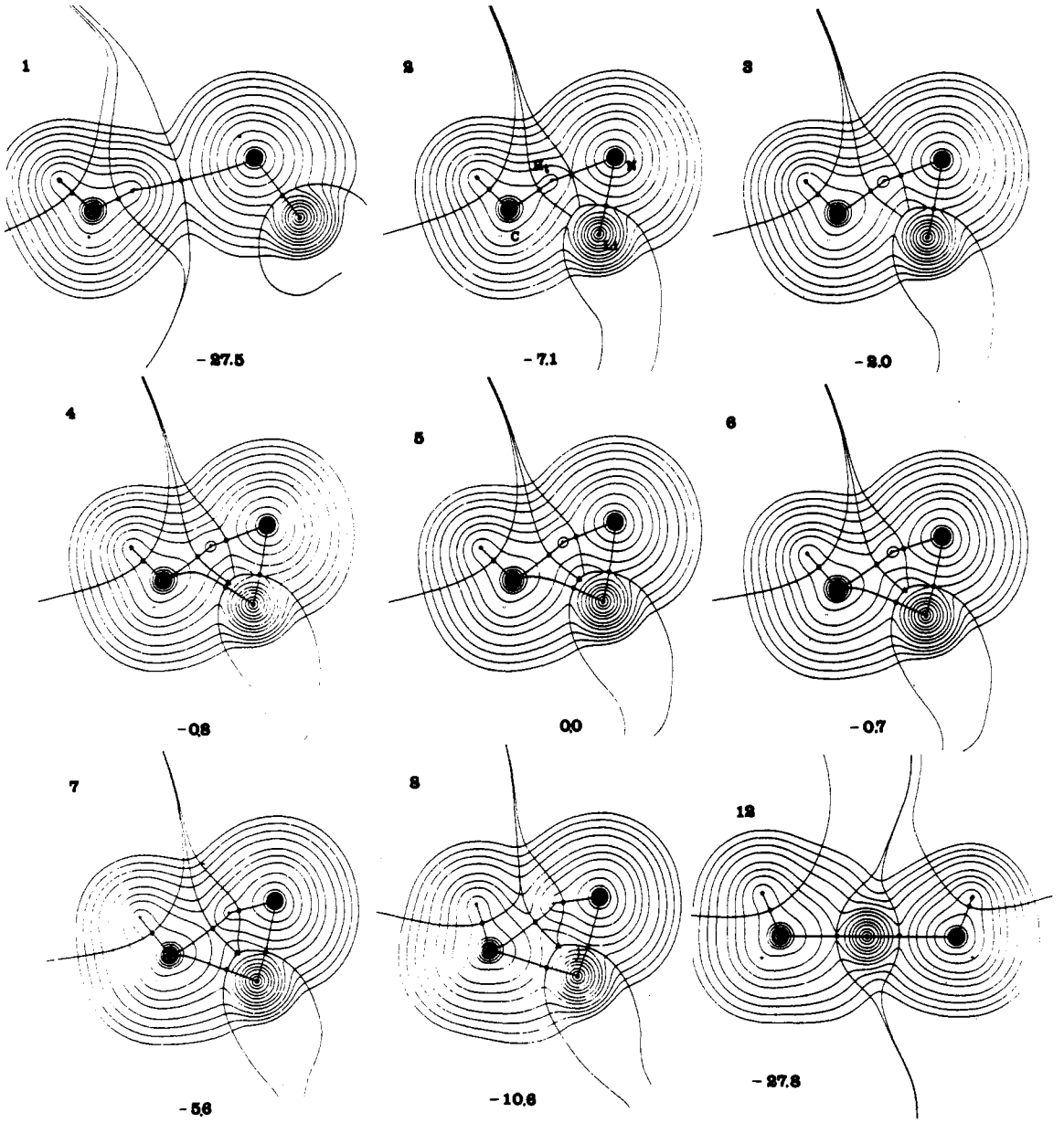

Figure 6. Contour maps of the electronic charge density overlaid with bond paths and interatomic surfaces for structures along the reaction pathway. The energies (in kcal/mol) relative to the transition state **5** are given. Note how the interatomic surfaces define recognizable reactant and product groups in the early and late stages of the reaction. The value of the outer contour is 0.001 au and the contours increase in value inwards from this value in the order 2×10^n, 4×10^n, and 8×10^n and n beginning at −3.

TABLE III: Properties of Reactants and Products, 6-31G**

molecule	energy, au	bond A–B	R(A–B), Å	q(A), e	q(B), e	ρ_b, e bohr^{-3}	$\nabla^2\rho_b$, e bohr^{-5}	magnitude of charge concns in VSCC of C and N ($-\nabla^2\rho$) bonded	nonbonded
CH_4	−40.201 70	C–H	1.084	+0.246	−0.061	0.2855	−1.0539	1.188	
NH_2Li	−63.049 91	N–H	1.002	−1.547	+0.311	0.3481	−1.7751	1.615	2.236[a]
		N–Li	1.748	−1.547	+0.927	0.0558	+0.4308		
CH_3Li	−47.020 99	C–H	1.092	−0.505	−0.132	0.2689	−0.9024	0.990	
		C–Li	1.999	−0.505	+0.903	0.0424	+0.2086	0.869	
NH_3	−56.195 54	N–H	1.001	−1.119	+0.373	0.3581	−1.9375	1.911	3.211[b]

Changes in Atomic Populations and Energies between Reactants and Products[a]

	C	N	H[b]	Li	H_{CH_3}	H_{NH_2}	Σ
$\Delta N(\Omega)$, e	+0.750	−0.428	−0.434	+0.024	+0.071	−0.062	+0.0006
$\Delta E(\Omega)$, kcal mol^{-1}	−12.3	−73.2	+108.7	−2.3	−10.0	+15.6	+22.1

[a] The two lone-pairs of amide ion. [b] The lone pair of ammonia. [c] Differences are reported as products − reactants. [d] The transferred hydrogen.

the valence shell of the anionic fragment. In methyllithium, there is a single relatively broad and diffuse bonded charge concentration completely localized within the basin of the carbon atom linking the C and Li nuclei. Consequently, the C–Li bond has little directional character, the Li being easily pushed aside making the bonded charge concentration susceptible to electrophilic attack. The reverse of reaction 1 corresponds to the attack of this bonded charge concentration by an acidic hydrogen of ammonia.

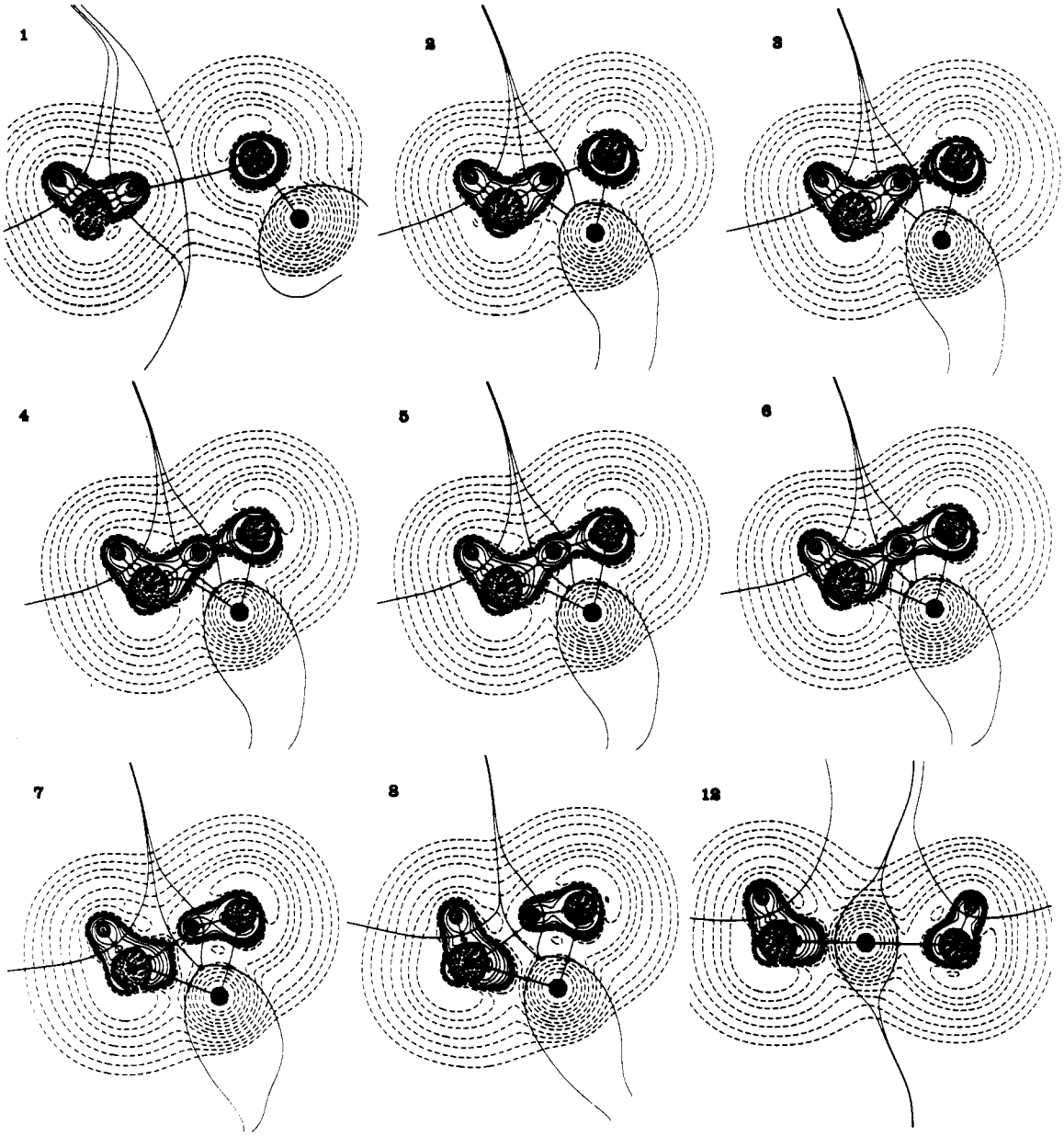

Figure 7. Contour displays of the Laplacian of ρ for structures along the reaction pathway. Solid contours denote regions of charge concentration, $\nabla^2\rho < 0$, and dashed contours regions of charge depletion, $\nabla^2\rho > 0$. There is a small spikelike region of charged concentration at the Li, C, and N nuclei surrounded by a shell of charge depletion, which together define the first quantum shell for these atoms. The C, N, and H atoms exhibit a valence shell charge concentration, the Li does not. Note the progressive broadening of the bond charge concentration on C that is shared with the transferred H, and its motion around the carbon core toward the approaching Li atom. Note as well the formation of the bridge of charge concentration between H and N leading up to the transition state and the eventual scission of the original bridge between C and H after the transition state.

The topology of the Laplacian distribution function recovers the shell structure of an atom, free or bound.[15,19,20] Each quantum shell appears as a shell of charge concentration, $\nabla^2\rho < 0$, bounded by one of charge depletion, $\nabla^2\rho > 0$. Of particular importance is the outer or valence shell charge concentration (VSCC) which for a bound atom, exhibits maxima which parallel in number, size, and relative location the localized electron pairs assumed in the Lewis model.[15,21] In agreement with the Lewis model, the VSCCs of carbon and nitrogen in methane, methyllithium, and ammonia exhibit four local charge concentrations (i.e., local maxima in $-\nabla^2\rho_b$) directed along tetrahedral or near tetrahedral axes: four bonded maxima for carbon in methane and methyllithium and three bonded and one nonbonded (lone pair) maxima for nitrogen in ammonia. The sizes of these charge concentrations are given in Table III. The lithium amide molecule is nearly planar, and the VSCC of nitrogen in this molecule is unusual. There are again four local charge concentrations, but only two are bonded maxima, those associated with the protons, and the remaining two are nonbonded (lone pair) maxima with the bond path to the lithium atom nearly bisecting the angle formed by the two nonbonded charge concentrations and the N nucleus. In this manner the positively charged Li is maximally removed from the similarly charged protons, a situation achieved by the C_{3v} geometry both anticipated and found in methyllithium.

Changes in the Atomic and Bond Properties along the Reaction Pathway

The energy quoted for each map in Figure 6 is relative to the energy of the transition state, the central map in Figures 6 and 7. The molecular graphs and interatomic surfaces overlaid on these maps together with the atomic properties and values of ρ_b and $\nabla^2\rho_b$ collected in Table IV provide an atomic view of the course of the reaction. Table IV also includes the changes in the atomic energies and populations of the reactants for the formation of the transition state. Note the blank entries for bond critical point data indicating that initially there is no C–Li bond and that the C–H bond ceases to exist after structure **10**.

TABLE IV: Atomic and Bond Properties for Structures on Reaction Path[a]

					ρ_b				$\nabla^2\rho_b$		
	ΔE	R(CH)	R(HN)	q(H)	C–H	N–H	C–Li	N–Li	C–H	N–H	C–Li
1	–27.5	2.074	5.408	–0.011	0.289	0.006		0.055	–1.096	+0.016	
2	–7.1	2.296	3.159	+0.322	0.222	0.080		0.045	–0.765	+0.118	
3	–2.0	2.513	2.728	+0.411	0.169	0.110		0.043	–0.447	–0.005	
4	–0.8	2.598	2.633	+0.439	0.151	0.125	0.025	0.042	–0.341	–0.100	+0.168
5	0.0	2.738	2.491	+0.470	0.126	0.152	0.025	0.041	–0.196	–0.320	+0.159
6	–0.7	2.878	2.354	+0.498	0.105	0.184	0.026	0.041	–0.085	–0.619	+0.153
7	–5.6	3.209	2.091	+0.547	0.069	0.265	0.030	0.036	+0.051	–1.310	+0.155
8	–10.6	3.502	2.054	+0.536	0.045	0.283	0.032	0.036	+0.074	–1.489	+0.150
9	–22.7	4.946	1.918	+0.463	0.013	0.346	0.039	0.020	+0.012	–1.923	+0.187
10	–23.3	5.023	1.914	+0.456	0.012	0.347	0.040	0.020	+0.033	–1.924	+0.187
11	–23.3	5.026	1.914	+0.453		0.347	0.040	0.020		–1.924	+0.187
12	–27.8	8.653	1.896	+0.443		0.355	0.041	0.024		–1.959	+0.191

Changes in Atomic Populations and Energies between Reactants and Transition State[b]

	C	N	H	Li	H_{CH_3}	H_{CH_3}[c]	H_{NH_2}	Σ
$\Delta N(\Omega)$, e	+0.559	–0.112	–0.532	+0.004	+0.013	+0.074	–0.040	+0.0004
$\Delta E(\Omega)$, kcal/mol	–95.6	–74.5	+178.8	+8.2	+1.6	–9.3	+13.2	+26.2

[a] Structures numbered in Figures 7–9. Structure 5 is the transition state. [b] Differences reported as transition state – reactants. [c] There are two such hydrogen atoms.

The reaction is initiated by the formation of a weak hydrogen bond between a hydrogen on methane and one of the two nonbonded charge concentrations on the nitrogen of the amide, structure **1**. A hydrogen bond is a result of an interaction between two closed-shell systems and it exhibits the characteristics of such an interaction: ρ_b low in value and $\nabla^2\rho_b > 0$.[15,22] The values of ρ_b in Table IV indicate that the progressive weakening of the C–H bond is paralleled by a strengthening of the N–H bond as the separation between the C and N nuclei is decreased. Not until the reaction structure is within 2 kcal mol^{-1} of the transition state does the N–H interaction change from a closed-shell to a shared interaction. From this point on there is a rapid increase in the amount of electronic charge in the N–H bond and in the extent of its contraction towards the N–H bond path, Figure 7. Thus in **5**, the transition-state structure, ρ_b(N–H) > ρ_b(C–H) and $\nabla^2\rho_b$ is more negative for N–H than it is for C–H. This weakening of the C–H bond reduces the binding of the associated C–H bonded charge concentration which polarizes towards the Li atom and at some geometry between structures **3** and **4**, a bond path is formed between the lithium and carbon atoms to yield the ring structure found in the transition state.

The movement of the N–H zero-flux interatomic surface toward the proton as the reaction progresses leads to a considerable reduction in the population of the hydrogen, particularly in the initial stages of the reaction where its nonbonded charge is transferred to the nitrogen atom. The net charge on the hydrogen atom transferred in the reaction must change from a small net negative value of –0.06 e in methane to a positive value of +0.37 e in ammonia. The charge on this atom in the transition state is +0.47 e; its population being less when bonded to both C and N than when bonded to just N in the product molecule; that is, the charge on the transferring hydrogen is not a composite or blend of reactant and product but is a distinct and more ionic entity. The electronic charge lost by H and N is transferred to the methyl group, primarily to the carbon which possesses a net charge of –0.31 e in the transition state. There is a reduction of 0.11 e in the population of N in attaining the transition state because of the partial transfer of the Li binding to the carbon atom. As detailed above, the binding of Li is ionic to both N and C. Thus the charge lost by N is passed directly to C, the population on Li changing by only 0.004 e in reaching the transition state.

The considerable charge reorganization along the C–H–N bridge of atoms in the ring structure leads to significant changes in their energies. The loss of ≈0.5 e by the hydrogen atom leads to a large energy increase, Table IV. For a bound hydrogen atom, the binding energy per electronic charge, the ratio E(H)/N(H), decreases in value across a short row of the periodic table. This is due to the increase in the tightness of the binding of electronic charge resulting from the increase in the nuclear charge of the atom to which the hydrogen is bound. This ratio equals –0.610 au in methane, –0.757 au in ammonia, and its value for the hydrogen transferred in the transition state is intermediate, equaling –0.668 au. Both the carbon and nitrogen atoms are substantially stabilized in the transition state, Table IV. The carbon is stabilized as a consequence of its substantial gain in electronic charge and its emerging bond to Li and in spite of the weakening of its bond to H. The nitrogen is stabilized because of its bond formation to hydrogen and because of an increase in the tightness of binding of its charge density, E(N)/N(N) decreasing to –6.49 au from its value of –6.40 in the amide. This increase in binding is reflected in the changes in the Laplacian distribution of N which in the transition state possesses four bonded charge concentrations, three shared with the hydrogens and one with the lithium, as opposed to the two bonded and two nonbonded concentrations found in $LiNH_2$. The magnitude of the bonded charge concentrations (as given by the Laplacian) shared with the protons in the amide group increases to 1.72 au in the transition state (compare with data in Table III), while the two initially nonbonded maxima in the amide increase to 2.28 and 2.42 au, respectively, on bonding to H and to the lithium.

As a consequence of the small change in population for the lithium atom through the course of the reaction, its energy changes are small, increasing by 8.2 kcal mol^{-1} in forming the transition state and being stabilized by 2.3 kcal mol^{-1} in the product methyllithium.

In the transition state, the VSCCs of the methyl and amide groups are bridged by the charge concentration carried by the shared hydrogen atom H to yield one continuous region of charge concentration. The magnitudes of the bonded charge concentrations in the VSCCs of N and C linking H are 2.24 and 1.19 au in the reactants, Table III. Downhill from the energy maximum, the bridge of charge concentration linking H to the bonded maximum on carbon is rapidly weakened and when the energy has decreased by 5.6 kcal mol^{-1}, structure **7**, the bridge is broken and $\nabla^2\rho_b > 0$ for the C–H bond. The bonded charge concentration on carbon is equally shared by both the transferred hydrogen and the lithium atoms in this structure, while in the succeeding ones it assumes the characteristics associated with the bonded maximum in methyllithium. The magnitude of the bonded maximum with Li in the VSCC of carbon in structure **8** is 0.94 au, compared with 0.87 au in methyllithium. The C–H bond is not broken and the ring structure opened until the energy of the system is within 4.5 kcal mol^{-1} of the product complex, between structures **10** and **11**. Methyllithium and ammonia are

recognizable components of the final structure, **12**, shown for the reaction pathway. Structure **12** is the complex (Ib) formed by the interaction of the lithium of methyllithium and the nonbonded charge concentration on the nitrogen atom in ammonia. The lithium atom is bonded to both the carbon and the nitrogen atoms by closed-shell interactions in this structure with parameters for the C–Li bond critical point only slightly reduced in value from those found for the isolated methyllithium.

The quadrupole ion model of the transition state provides a rationalization of its geometry and accounts for the insensitivity of this geometry to electron correlation. However, note that the values of ρ_b for the bonds to the hydrogen being transferred in the transition state, while substantially less than for normal C–H and N–H bonds, are greater than those of typically ionic bonds such as those to lithium. The displays of the electron density and its Laplacian, structure **5** in Figures 6 and 7, together with theory enable one to draw a more detailed physical picture of the transition state. The net charges on the four groups in the transition state are $q(CH_3) = -0.66$ e, $q(NH_2) = -0.73$ e, $q(Li) = +0.92$ e, and $q(H) = +0.47$ e. The properties of ρ and of the Laplacian support the conclusion that Li is indeed bound as an ion to the remainder of the complex. Hydrogen is bound in a closed-shell ionic interaction to N or to C in structures on either side of the transition state, to N in **3** and to C in **7**, along with a second shared covalent interaction to C or N. However, in the transition state it is clear that the proton, while possessing a substantial net charge, is bound by weak shared interactions by both C and N. The reader may readily appreciate the extent to which the flow of charge concentrations depicted in the sequence of Laplacian maps mimics the movement of electron pairs that a chemist would indicate with curved arrows. The nonbonded charge concentration on N flows out to and encompasses the proton, thereby displacing the original C–H bonded concentration which is simultaneously withdrawn from the proton and used to bind the Li ion.

Conclusion

The proton-transfer reaction of lithium amide with methane is adequately represented at the Hartree–Fock level. At HF/6-31G* (6-31G**), without zero-point energy corrections, the first intermediate is a weak complex, 3.4 (1.2) kcal mol^{-1} more stable than the separated $LiNH_2 + CH_4$. The proton transfer transition state is 31.7 (27.5) kcal mol^{-1} above this complex and yields a new complex, methyllithium with lithium complexed to ammonia, 29.1 (27.9) kcal mol^{-1} more stable than the transition state. Separation of this complex into NH_3 and $LiCH_3$ requires 24.1 (23.6) kcal mol^{-1}; these products are 23.4 (22.0) kcal mol^{-1} less stable than $LiNH_2 + CH_4$. The structure of the transition state is changed only slightly by MP2 correlation or by solvating the Li with one NH_3 molecule. The transition state is highly polar and can be modeled approximately as a quadruple ion of NH_2^-, CH_3^-, Li^+, and H^+. The reaction can be followed by the electron density function that shows the formation and breaking of bonds (bond paths) and that characterizes the electronic properties of the constituent atoms.

Acknowledgment. This research was supported in part by NSF grant CHE 87-21134 and by the UCSD Supercomputer Center.

References and Notes

(1) (a) Wakefield, B. J. *The Chemistry of Organolithium Compounds*; Pergamon: Oxford, 1974. (b) Mallan, J. M.; Bebb, R. L. *Chem. Rev.* **1969**, *69*, 693. (c) Gilman, H.; Morton, J. W., Jr. *Org. React. (N.Y.)* **1954**, *8*, 258.

(2) (a) Streitwieser, A., Jr.; Caldwell *J. Am. Chem. Soc.* **1965**, *87*, 5383. (b) Streitwieser, A., Jr.; Caldwell, R. A.; Lawler, R. G.; Ziegler, G. R. *J. Am. Chem. Soc.* **1965**, *87*, 5383. (c) Streitwieser, A., Jr.; Young, W. R.; Caldwell, R. A. *J. Am. Chem. Soc.* **1969**, *91*, 527. (d) Streitwieser, A., Jr.; Caldwell, R. A.; Young, W. R. *J. Am. Chem. Soc.* **1969**, *91*, 529. (e) Streitwieser, A., Jr.; Young, W. R. *J. Am. Chem. Soc.* **1969**, *91*, 529. (f) Streitwieser, A., Jr.; Ziegler, G. R. *J. Am. Chem. Soc.* **1969**, *91*, 5081. (g) Streitwieser, A., Jr.; Maskornick, M. J.; Ziegler, G. R. *Tetrahedron Lett.* **1971**, *42*, 3927. (h) Maskornick, M. J.; Streitwieser, A., Jr. *Tetrahedron Lett.* **1972**, *17*, 1625. (i) Streitwieser, A.; Dixon, R. E.; Williams, P. G.; Eaton, P. E. *J. Am. Chem. Soc.* **1991**, *113*, 357–8. (j) Dixon, R. E.; Streitwieser, A. *J. Org. Chem.* **1992**, *57*, 6125–8.

(3) Kaufmann, E.; Schleyer, P. v. R. *J. Comp. Chem.* **1989**, *10*, 437. Kaufmann, E.; Sieber, S.; Schleyer, P. v. R. *J. Am. Chem. Soc.* **1989**, *111*, 121–5.

(4) (a) Roothaan, C. C. J. *Rev. Mod. Phys.* **1951**, *23*, 69. (b) Hall, G. G. *Proc. R. Soc. London* **1951**, *A205*, 541.

(5) Davidon–Fletcher–Powell algorithm: (a) Davidon, W. C. *Comput. J.* **1968**, *10*, 406. (b) Fletcher, R.; Powell, M. J. D. *Comput. J.* **1963**, *6*, 163. (c) Poppinger, D. *Chem. Phys. Lett.* **1975**, *34*, 332. Schlegel algorithm: (d) Schlegel, H. B. J. *J. Comput. Chem.* **1982**, *3*, 234.

(6) *Gaussian 86*: Frisch, M. J.; Binkley, J. S.; Schlegel, H. B.; Raghavachari, K.; Melius, C. F.; Martin, R. L.; Stewart, J. J. P.; Bobrowicz, F. W.; Rohlfing, C. M.; Kahn, R. L.; DeFrees, D. J.; Seeger, R.; Whiteside, R. A.; Fox, D. J.; Fleuder, E. M.; Pople, J. A. Carnegie-Mellon Quantum Chemistry Publishing Unit: Pittsburgh, PA. *Gaussian 88*: Frisch, M. J.; Head-Gordon, M.; Schlegel, H. B.; Raghavachari, K.; Binkley, J. S.; Gonzalez, C.; Defrees, D. J.; Fox, D. J.; Whiteside, R. A.; Seeger, R.; Melius, C. F.; Baker, J.; Martin, R. L.; Kahn, L. R.; Stewart, J. J. P.; Fluder, E. M.; Topiol, S.; Pople, J. A. Gaussian Inc.: Pittsburgh, PA.

(7) GAMESS version 7, Jan 1990: Dupuis, M.; Spangler, D.; Wendoloski, J. J.; Schmidt, M. W.; Elbert, S. T., North Dakota State University, Fargo, ND 58015, and Ames Laboratory—USDOE, Iowa State University, Ames, IA 50011. For current information see: *QCPE Bull.* **1992**, *12*, 78.

(8) *The Carnegie-Mellon Quantum Chemistry Archive*, 3rd ed.; Whiteside, R. A., Frisch, M. J., Pople, J. A., Eds.; Department of Chemistry, Carnegie-Mellon University, Pittsburgh, PA, 1983.

(9) (a) Baker, J. J. *J. Comput. Chem.* **1986**, *7*, 385. (b) Simons, J.; Jorgensen, P.; Taylor, H.; Ozment, J. *J. Phys. Chem.* **1983**, *87*, 2745.

(10) Biegler-König, F. W.; Bader, R. F. W.; Tang, T.-H. *J. Comput. Chem.* **1982**, *3*, 317.

(11) Streitwieser, A., Jr. *Acc. Chem. Res.* **1984**, *10*, 353.

(12) See for example: DeFrees, D. J.; Levi, B. A.; Pollack, S. K.; Hehre, W. J.; Binkley, J. S.; Pople, J. A. *J. Am. Chem. Soc.* **1979**, *101*, 4085.

(13) (a) Shepard, R. In *Ab Initio Methods in Quantum Chemistry*, Part II; Lawley, K. P., Ed.; Wiley: New York, 1987; p 63. (b) Ruedenberg, K.; Schmidt, M. W.; Dombek, M. M.; Elbert, S. T. *Chem. Phys.* **1982**, *79*, 41, 51, 65.

(14) Kaufmann, E.; Tidor, B.; Schleyer, P. v. R. *J. Comput. Chem.* **1986**, *7*, 334.

(15) Bader, R. F. W. *Atoms in Molecules—A Quantum Theory*; Oxford University Press: Oxford, U.K., 1990.

(16) Bader, R. F. W.; Slee, T. S.; Cremer, D.; Kraka, E. *J. Am. Chem. Soc.* **1983**, *105*, 5061.

(17) For example, cf.: (a) Streitwieser, A., Jr.; Williams, J. W.; Alexandratos, S.; McKelvey, J. M. *J. Am. Chem. Soc.* **1976**, *98*, 4778. (b) Streitwieser, A., Jr. *J. Organomet. Chem.* **1978**, *156*, 1; Kaufmann, E.; Raghavachari, K.; Reed, A. E.; Schleyer, P. v. R. *Organometallics*, **1988**, *7*, 1597.

(18) (a) Boyd, R. J.; Choi, S. C.; *Chem. Phys. Lett.* **1985**, *120*, 80. (b) Choi, S. C.; Boyd, R. J.; Knop, O. *Can. J. Chem.* **1987**, *65*, 1109.

(19) Bader, R. F. W.; Essén, H. J. *J. Chem. Phys.* **1984**, *80*, 1943.

(20) (a) Sagar, R. P.; Ku, A. C.; Smith, V. H.; Sinas, A. M. *J. Chem. Phys.* **1988**, *88*, 4367. (b) Shi, Z.; Boyd, R. J.; *J. Chem. Phys.* **1988**, *88*, 4375.

(21) Bader, R. F. W.; McDougall, P. J.; Lau, C. D. H. *J. Am. Chem. Soc.* **1984**, *106*, 1594.

(22) Carroll, M. T.; Bader, R. F. W. *Mol. Phys.* **1988**, *65*, 695.